Sensitivity and Source of Amine-Proton Exchange and Amide-Proton Transfer Magnetic Resonance Imaging in Cerebral Ischemia

Xiaopeng Zong, Ping Wang, Seong-Gi Kim, and Tao Jin*

Purpose: Amide-proton transfer (APT) and amine–water proton exchange (APEX) MRI can be viable to map pH-decreasing ischemic regions. However, their exact contributions are unclear.
Methods: We measured APEX- and APT-weighted magnetization transfer ratio asymmetry (denoted as APEXw and APTw), apparent diffusion coefficient, T_2, and T_1 images and localized proton spectra in rats with permanent middle cerebral artery occlusion at 9.4 T. Phantoms and theoretical studies were also performed.
Results: Within 1-h postocclusion, APEXw and APTw maps showed hyperintensity (3.1% of M_0) and hypointensity (−1.8%), respectively, in regions with decreased apparent diffusion coefficient. Ischemia increased lactate and gamma aminobutyric acid concentrations, but decreased glutamate and taurine concentrations. Over time, the APEXw contrast decreased with glutamate, taurine, and creatine, whereas the APTw contrast and lactate level were similar. Phantom and theoretical studies suggest that the source of APEXw signal is mainly from proteins at normal pH, whereas at decreased pH, gamma aminobutyric acid and glutamate contributions increase, inducing the positive APEXw contrast in ischemic regions. The APTw contrast is sensitive to lactate concentration and pH, but contaminated from contributions of the faster APEX processes.
Conclusion: Positive APEXw contrast is more sensitive to ischemia than negative APTw contrast. They may provide complementary tissue metabolic information. **Magn Reson Med 71:118–132, 2014. © 2013 Wiley Periodicals, Inc.**

Key words: cerebral ischemia; apparent diffusion coefficient; amide; amine; chemical exchange saturation transfer; spin locking; stroke; MR spectroscopy

INTRODUCTION

Magnetic resonance imaging (MRI) has become one of the most useful imaging techniques in acute brain ischemia for accurate diagnosis, evaluating disease progression, therapeutic decision making, and monitoring treatment response. Many modalities, such as diffusion, perfusion, and T_1- and T_2-weighted MRI, have been applied in ischemia studies to probe different aspects of physiological information. However, MRI techniques are still under development in several important aspects of ischemia diagnosis, such as the detection of penumbra and determination of the onset time of ischemia.

It has been reported that chemical exchange (CE)-dependent contrasts such as the amide-proton transfer (APT)-weighted magnetization transfer (MT) ratio asymmetry (MTR_{asym}) (denoted as APTw) and the on-resonance $T_1\rho$, the spin–lattice relaxation time in the rotating frame, may offer unique information about ischemic tissue microenvironment, thus complementing conventional contrasts, such as diffusion and perfusion. The APTw signal is based on the slow proton exchange between water and the backbone amide protons of proteins and peptides with rates around 10–30 s^{-1} and is sensitive to tissue acidification as well as protein concentrations (1). APTw has been proposed as a potential biomarker for the ischemic penumbra; however, the in vivo sensitivity is relatively low being only 1–3% of the fully relaxed water signal (2). On-resonance spin locking (SL) is another CE-sensitive technique that has been reported as a sensitive biomarker of early ischemia (3,4). The quantitative change of ischemic $T_1\rho$ showed strong time dependence and may be able to indicate the onset time of stroke (5). Unfortunately, large SL pulse power, i.e., $B_1 \geq 0.5$ G, is necessary for the detection of $T_1\rho$ change, which may severely limit its application. On-resonance $T_1\rho$ is nonspecific and has contributions from all exchangeable protons as well as other molecular relaxation mechanisms. Recently, we have reported that the amine–water proton exchange (APEX)-weighted MTR_{asym} signal (APEXw) may be explored as a potential sensitive biomarker of stroke (6). APEXw probes the CE of the relatively fast exchanging amine protons, based on an off-resonance SL technique. Off-resonance SL is similar to the widely used CE saturation transfer (CEST) technique (7) but with a higher sensitivity than CEST when the angle between the effective field of the saturation pulse in the rotating frame, and the B_0 field becomes large (8). Compared to the on-resonance SL, the off-resonance SL can achieve similar effective SL field at much smaller B_1 (e.g., ~0.1 G), and the asymmetry analysis can greatly reduce the contribution from non-CE relaxations. In our initial ischemia studies, the APEXw contrast showed enhanced sensitivity compared to the APTw, and different spatiotemporal characteristics from APTw and apparent diffusion coefficient (ADC), suggesting that the APEXw and the APTw contrasts have different physiological origins.

In this study, we carried out multiparametric MRI and magnetic resonance spectroscopy (MRS) studies in rats with permanent middle cerebral artery occlusion (MCAO) to further investigate the physiological sources and sensitivities

Neuroimaging Laboratory, Department of Radiology, University of Pittsburgh, Pittsburgh, Pennsylvania, USA.

Grant sponsor: NIH; Grant numbers: EB008717; EB003324; EB003375; NS44589.

*Correspondence to: Tao Jin, Ph.D., Department of Radiology, University of Pittsburgh, 3025 E Carson Street, Room 156, Pittsburgh, PA 15203. E-mail: taj6@pitt.edu

Received 18 September 2012; revised 19 December 2012; accepted 19 December 2012
DOI 10.1002/mrm.24639
Published online 11 February 2013 in Wiley Online Library (wileyonlinelibrary.com).

of the APTw and APEXw contrasts. ADC, T_2, T_1, APTw, and APEXw signals and metabolite concentrations were repeatedly measured within 4.5 h after the onset of MCAO. To better understand the sources of the in vivo APEXw and APTw contrasts, the APEXw and APTw signals were also measured in phantoms of metabolite and protein solutions under physiological pH values, and theoretical analyses of the APEXw and APTw signals were performed with a two-pool exchange model. Throughout the article, APEXw and APTw will be used to denote the MTR_{asym} measured using the pulse sequences described later, even if the sample contains no amine or amide protons.

METHODS

All animal and phantom experiments were performed on a 9.4 T magnet equipped with an actively shielded 12-cm gradient system (Magnex, UK), interfaced to a Unity INOVA (Varian, Palo Alto, CA) or DirectDrive 2 console (Agilent, Santa Clara, CA). Detunable volume excitation (6.4-cm diameter) and surface receiver coils (2.2-cm diameter) (Nova Medical, MA) were used for animal studies, while a 3.8-cm ID quadrature volume coil (Rapid Biomedical, OH) was used for phantom studies. All images were obtained with a spin-echo echo planar imaging (EPI) sequence.

Animal Experiments

Animal Preparation

Sixteen male Sprague–Dawley rats weighing 280–410 g were studied with approval by the Institutional Animal Care and Use Committee at the University of Pittsburgh. The animals were anesthetized with isoflurane (5% for induction and 2% during surgery) in a mixture of O_2 and air gases with the O_2 concentration kept at 30% throughout the experiment. The right femoral vein and artery were catheterized to deliver pancuronium bromide (0.2 mg/kg/h) and maintenance fluid and to monitor the arterial blood pressure, respectively. After catheterization, MCAO was carried out to induce permanent ischemia in the left hemisphere (9). Briefly, an incision was made on the midline of the neck. The left common carotid artery, internal carotid artery, and external carotid artery were isolated and common carotid artery and external carotid artery ligated. A 4-0 monofilament nylon suture coated with silicon rubber (Doccol Corp., CA) was inserted from the external carotid artery into the internal carotid artery to occlude the origin of the middle cerebral artery. After surgery, the isoflurane level was reduced to 1.3–1.5% during MRI scans. The dynamic blood pressure and end-tidal CO_2 were monitored. End-tidal CO_2 level was kept within 3.0–4.0%, and the rectal temperature was maintained at $37.2\pm0.5^{\circ}C$ using a feedback-controlled heating pad (Digi-Sense Temperature Controller R/S, Cole-Parmer, IL).

Animal MR Experiments

ADC, APEXw, and APTw maps, R_2, and R_1 maps, and water-suppressed localized proton spectra were repeatedly measured between 30 min and ~5 h after the onset of MCAO. Among the 16 animals studied, one animal had ischemia on both hemispheres and was excluded from further data analysis. ADC and APEXw maps were measured in the remaining 15 rats, whereas APTw, R_2 map, R_1 map, and proton spectra were measured in 10, 6, 5, and 10 rats, respectively. Common imaging parameters were field of view=3.2 × 3.2 cm^2, slice thickness=2 mm, in-plane matrix=64 × 64, and the number of consecutive slices without gap=4.

Conventional MRI experiments. ADC maps were obtained using a diffusion-weighted spin-echo EPI sequence, with a low b value of 5 s/mm^2 applied along one axis, and a high b value of 1200 s/mm^2 applied along six different directions. Echo time (TE)/pulse repetition time (TR)=40/2800 ms, and number of averages (NEX)=8. Images with the six high b values were averaged together. Then, ADC was calculated as $ADC = \ln(S_1/S_2)/(b_2 - b_1)$, where S_1 and S_2 are the image intensities at b_1=5 s/mm^2 and b_2=1200 s/mm^2, respectively.

T_2-weighted images were measured with a double spin-echo EPI sequence with 6 TE values between 28 and 72 ms, TR=12 s, and NEX=3. R_2 maps were calculated from nonlinear least-square fitting of a single exponential decay to the image intensity versus TE plots. T_1-weighted images were measured with an inversion-recovery sequence. Fifteen inversion times (TI) between 10 ms and 10 s were used, and a 10-s delay was inserted between EPI acquisition and the following inversion pulse to allow complete relaxation of longitudinal magnetization. To obtain R_1 maps, k-space data were subtracted by the data at the longest TI for obtaining unipolar data and then Fourier transformed to the image space (10). The image intensity versus TI data was fitted by $s(\mathrm{TI}) = a + c \cdot \exp(-R_1\mathrm{TI})$, where a and c are constants.

CE-sensitive MRI experiments. The APEXw images were measured with an off-resonance SL sequence (6). Parameters of the SL pulse were: 150-ms square pulse, 500-Hz irradiation power, and 2.5-ppm (amine frequency), −2.5-ppm (reference frequency), or 300-ppm (control frequency) frequency offset relative to the water proton resonance with respective NEX=30, 20, and 3. Although amine protons from most amino acids and proteins peak at 2.8–3 ppm (7), 2.5 ppm was empirically chosen from our preliminary studies for maximizing the APEXw signal at normal brain cortex with a relatively short SL pulse duration. Based on previous theoretical results, the optimal SL duration for a fixed B_1 is approximately proportional to $1/\sin^2\theta$, which decreases at smaller frequency offset, where θ is the angle between the effective SL field and B_0 (6). TE/TR=28/6300 ms. APEXw maps were calculated from the SL scans as $APEXw = SLR_{asym} = (S_{-2.5ppm} - S_{2.5ppm})/S_{300ppm}$, where subscripts indicate off-resonance irradiation frequencies.

APTw maps were measured following magnetization preparation with an off-resonance continuous wave pulse. Parameters of the continuous-wave pulses were: 3-s duration, 63-Hz irradiation power, 3.5 ppm (amide frequency), −3.5 ppm (reference frequency), and 300 ppm (control frequency) offset relative to the water proton resonance with respective NEX=12, 11, and 4. Following each slice acquisition, a 240-ms square pulse

with the same B_1 and offset was applied to approximately compensate for longitudinal relaxation during multislice imaging (11). The duration of the compensating pulse was empirically determined to maintain similar APT-weighted MTR_{asym} values at the cortex area between different slices. TE/TR = 28/7600 ms. APTw maps were calculated as $APTw=MTR_{asym}=(S_{-3.5ppm}-S_{3.5ppm})/S_{300ppm}$.

Localized proton spectroscopy. Water-suppressed localized ^1H spectra were measured with a short-TE localized stimulated-echo acquisition mode (STEAM) sequence (12). The pulse widths of the three asymmetric 90° radiofrequency (RF) pulses were 1.26, 1, and 1 ms, which correspond to an excitation spectral width of 5.4, 6.8, and 6.8 kHz, respectively. The frequency of the RF pulses was set roughly at the middle (2.85 ppm) of the interested frequency range of 1.3–4.0 ppm. Parameters were TE/TR=4/3000 ms, NEX=256, readout spectral width=4000 Hz, number of complex data points=2048, and the voxel size = 3 × 3 × 3 mm^3. Spectra were obtained from two regions: one ischemic region determined from the first ADC map obtained after MCAO and the other control region in the contralateral hemisphere. Ischemic spectra were acquired about hourly, and the control spectrum was measured ~5 h after MCAO onset. Before obtaining localized spectra, first- and second-order shimming were performed by the FASTMAP technique (13), resulting in the unsuppressed water line width of typically 12–16 Hz. Unsuppressed water spectrum was also acquired in the same voxels with NEX=6 for quantification. Four dummy scans were added to the beginning of both the water-suppressed and unsuppressed scans to ensure steady-state during acquisition.

To quantify metabolite concentrations, a macromolecule spectrum was measured in one rat starting 5 h after MCAO onset in a voxel of 4 × 4 × 4 mm^3 centered roughly at the lesion center. All parameters were the same except for TR of 4 s. To null the metabolite signals, an adiabatic inversion pulse was applied at the beginning of the sequence (14), and TI of 0.95 s was used, at which time the metabolite signals were mostly nulled, whereas the macromolecule magnetization was positive due to its much shorter T_1.

For each animal, all spectra on the lesion side were separated into three 80-min-period groups according to their acquisition times relative to the ischemia onset: 30–110 min, 110–190 min, and 190–270 min. Spectra within the same group were averaged together after phase correction for each spectrum. The spectroscopy data were analyzed with LCModel (15) implemented in MATLAB (Mathworks, MA). Apodization was not applied to the signal. The model spectra of the nine metabolites were simulated using the density matrix approach. The details of the simulation method are given in the Appendix. The steady-state signal intensities of the water and metabolites measured at TR=3 s were converted to the fully relaxed signal intensities at TE=0 and TR >> T_1 using relaxation times of water and metabolite protons: water T_1 measured in the same time window, metabolite T_1 of 1.4 s at 9.4 T (14), water T_2 of 38 ms (16,17), and metabolite T_2 of 144 ms for carbon-bound protons at 9.4 T (14). Due to the short TE value used, the small difference between the T_2 values on the lesion and contralateral sides is negligible for the quantification purpose. The first time point for Fourier transform of the time domain signal was carefully determined, so that no linear phase correction was needed. Nine simulated metabolite spectra glutamate (Glu), glutamine (Gln), gamma aminobutyric acid (GABA), *N*-acetylaspartate (NAA), lactate (Lac), creatine (Cr), phosphorylcholine (PCho), taurine (Tau), myo-Inositol (Ins), and the measured macromolecule spectrum were used as the basis set in the fitting. Because the peaks of Cr and phosphocreatine (PCr) were not well resolved in most cases, model spectrum for PCr was not included and the resulting Cr concentration thus represented that of total creatine (tCr). The metabolite concentration (in mol/g tissue) was obtained from the ratio (r) between the area under a best-fit metabolite spectrum in LCModel and that under the unsuppressed water spectrum as $= rf_w g_w/n$, where n is the number of observable protons in the metabolite molecule, f_w is the tissue water content (weight fraction), and g_w=0.111 mol/g is the proton concentration in water. f_w was assumed to be 77 and 79% on the contralateral and lesion sides, respectively (18).

Time Courses and Statistical Analyses

Regions of interest (ROIs) in two adjacent imaging slices were defined on the lesion and contralateral hemispheres to include all voxels in the EPI images matched with the corresponding STEAM voxels. In the five animals without spectroscopy data, ROIs were defined in a manner similar to choosing the STEAM voxels. As the B_0 inhomogeneity is very small within ROI (mean deviation 8–20 Hz), no correction of B_0 is necessary for our APTw and APEXw images. ROI-averaged ADC, R_2, R_1, APEXw, and APTw values were calculated. If multiple measurements were performed for each parameter within the same period of 30–110 min, 110–190 min, or 190–270 min, their results were averaged. To generate the group-averaged time courses of metabolite concentrations, the LCModel results for each metabolite (except for Lac and Gln) in each rat were included only if its Cramer-Rao lower bounds (CRLBs) for all three periods on the lesion side and on the contralateral side were less than 25%. For Lac, the inclusion criterion was CRLBs less than 25% for all three spectra on the lesion side, as the quantification of its concentration on the contralateral side is often unreliable (CRLB>25% for 7 out of 10 rats). The quantification of Gln was also unreliable in 25 out of the 40 cases due to the overlap of its peaks with those of Glu at 2.1 and 3.75 ppm, and its inclusion criterion was CRLB<25% in either the lesion or the contralateral side for each animal.

To evaluate the significance of imaging contrasts, paired *t*-tests were performed comparing the ROI-averaged data of the first period on the lesion and contralateral sides and also comparing the data averaged over the three periods on the lesion and contralateral sides. Similarly, to evaluate significance of metabolite concentration differences between the two hemispheres, paired *t*-tests

were performed comparing the concentrations of the first period on the lesion side and the concentrations on the contralateral side and also comparing the concentrations averaged over the three periods on the lesion side and the concentrations on the contralateral side. *P* values less than 0.05 after Bonferroni correction were considered significant. Further, significant time-dependent changes were evaluated by performing one-way analysis of variance (ANOVA) tests for differences of the metabolite concentrations and ROI-averaged imaging values among the three periods on the lesion side. For tests that gave *P* less than 0.01, paired *t*-tests were further carried out for comparing the first data point with the second and the third data points, and *P* values less than 0.05 were considered significant.

APEXw and APTw Measurements in Phantoms

Preparation

As the exchangeable amine group exists in metabolites as well as in proteins, two sets of phantoms, metabolites, and proteins, were measured at two pH values of 7.0 and 6.5. The intracellular pH is close to 7.0 under normal physiological conditions, whereas pH in ischemic brain regions was estimated to be 6.52±0.32 (1). For metabolite phantoms, 1× phosphate-buffered saline solutions (contains 10 mM phosphate) of 20 mM Glu, 20 mM Tau, 20 mM GABA, 20 mM Gln, 10 mM Cr and PCr each, and 10 mM Ins and NAA each were prepared. For protein phantoms, 1× phosphate-buffered saline solutions of 8% bovine serum albumin (BSA) and 8% egg white albumin (EWA) were prepared. The weight percentage of the two protein phantoms was chosen to roughly match the protein weight fraction of the brain (19). All solutions were doped with 0.1 mM of manganese chloride for shortening their T_1 and T_2 values (resulting $T_1 \approx 1.3$ s and $T_2 \approx 125$ ms for metabolite phantoms and $T_1 \approx 0.9$ s and $T_2 \approx 71$ ms for protein phantoms at 37°C). All chemicals were obtained from Sigma–Aldrich in St. Louis, MO. Prepared phantoms were transferred to plastic syringes (I.D.=8.9 mm) for imaging study.

MR Measurements

APEXw and APTw images were measured at 37°C with the same pulse sequences and the same sequence parameters as in the animal studies. A square ROI was defined within the image boundary of each solution phantom. Then, APEXw and APTw values were averaged over all the voxels within each ROI.

Theoretical Analyses of the APEXw and APTw Signals

Brain ischemia induces changes in CE rate, labile proton concentration, R_1, and R_2 which can all affect the observed APEXw and APTw signals. To gain a qualitative understanding of the dependences of APEXw and APTw on these four parameters, we analyzed a two-pool exchange model of a water proton pool exchanging with a second pool of dilute labile protons.

For APEXw studies, theoretical description of off-resonance SL was described in detail previously (6,8). In short, the water magnetization after a SL pulse with duration τ and frequency offset Ω from water is

$$M_{SL} = \frac{M}{M_0} = 1 - \left(1 - \frac{R_1 \cos\theta}{R_{1\rho}}\right)\left(1 - e^{-R_{1\rho}\tau}\right), \qquad [1]$$

where θ is the angle between the external field and the effective SL field in the rotating frame. $R_{1\rho}$ is given by (6,20)

$$R_{1\rho} = R_1 \cos^2\theta + (R_2 + R_{ex})\sin^2\theta, \qquad [2]$$

where R_1 and R_2 are the longitudinal and transverse relaxation rates in the absence of CE and R_{ex} is the contribution to the transverse relaxation rate from CE. In the case of dilute labile protons, i.e., asymmetric population limit, and also assuming $R_2 - R_1 << k$, R_{ex} is

$$R_{ex} \approx \frac{p_b \delta^2 k}{(\delta - \Omega)^2 + \omega_1^2 + k^2}, \qquad [3]$$

where δ is the offset of labile proton resonance from water proton frequency, k is the APEX rate, $\omega_1 = \gamma B_1$, p_b is the ratio of the labile proton and water proton concentrations, and Ω is the frequency of the SL pulse. If $\Omega = \delta$, R_{ex} increases with decreasing k when $k > \omega_1$ and decreases with decreasing k when $k < \omega_1$. The APEXw signal is equal to the difference of M_{SL} at Ω of -2.5 and 2.5 ppm.

The APTw signal can be derived from analytical solutions when the saturation pulse frequency (also denoted by Ω) satisfies $\Omega = \delta$ (21,22), and is negligible when $\Omega \neq \delta$ for slow exchange. However, for fast exchanging protons such as amine protons, their line width is broad by CE, and these protons can be partly saturated by the saturation pulse even when $\Omega \neq \delta$. In fact, it has been shown that at physiological pH values the CE signals from amine protons of glutamate (δ=3 ppm) can be detected within a wide RF offset range between about 0.5–5 ppm (8,23), which would contaminate the amide signal at 3.5 ppm. As the assumption of $R_2 - R_1 << k$ in deriving Eq. [3] is not satisfied for in vivo APT studies at 9.4 T, we calculated the APTw signal with the numerical solution of the two-pool Bloch–McConnell equations (24,25). In particular, the contribution of amine protons to the APTw signal was calculated for $\Omega \neq \delta$.

Theoretical curves of APEXw and APTw versus R_1, R_2, k, and p_b were calculated. Ω, ω_1, and τ were chosen to be the same as in the experiments: Ω=6238 rad s^{-1} (=2.5 ppm), ω_1=3142 rad s^{-1} (=500 Hz), and τ=0.15 s for APEXw and Ω=8797 rad s^{-1} (= 3.5 ppm), ω_1=396 rad s^{-1} (=63 Hz), and τ=3 s for APTw. The labile proton offset was set to δ=3.0 ppm (from amine) or 3.5 ppm (from amide) for APTw calculations. Only δ=3.0 ppm was used for APEXw calculations, as our imaging parameters were tuned to intermediate exchange rates, and amide protons with slow exchange rates (e.g., 10–30 s^{-1}) do not induce significant APEXw signal. For both APEXw and APTw analyses, the default R_1, R_2, and p_b values were set to 0.5 s^{-1}, 25 s^{-1}, and 0.003, respectively. The default value k was set to 8000 s^{-1} for δ=3.0 ppm or 30 s^{-1} for δ=3.5 ppm, which are representative values for the amine and amide protons. The default values of R_1 and

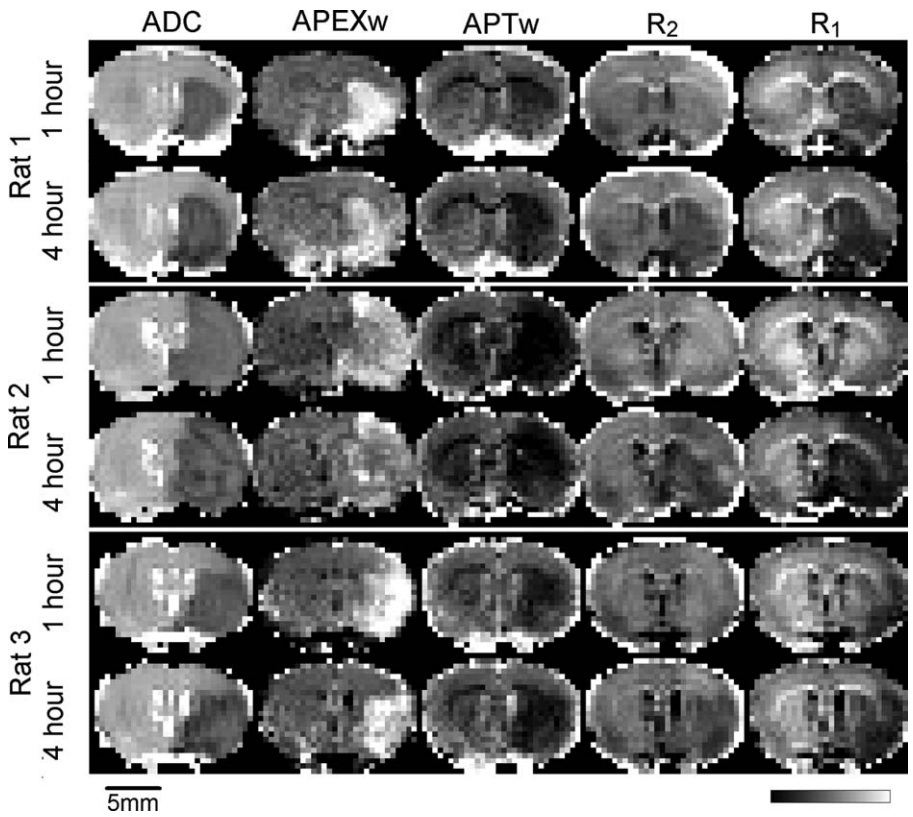

FIG. 1. ADC, APEXw, APTw, R_2, and R_1 maps in three representative rats at 1 and 4 h after the MCAO onset. Units for the gray color bars are given below the bars. The ranges of the gray bars are 0 – 0.9 × 10^{-3} mm^2/s, 0.05 – 0.15 s^{-1}, −0.1 – 0 s^{-1}, 15 – 35 s^{-1}, and 0.35 – 0.6 s^{-1}, for ADC, APEXw, APTw, R2, and R1, respectively.

R_2 were chosen to match the in vivo values, and the default values of k and p_b for APEXw were chosen such that the resulting APEXw roughly matches the measured value (12.6% of M_0) on the lesion hemisphere. For simplicity, R_1 and R_2 were assumed to be the same for both water and labile proton pools. One of the four parameters was varied and the remaining set to their default values to study the dependences of APEXw and APTw on that parameter.

RESULTS

Ischemia-induced Changes in Imaging and Proton Spectroscopic Data

Figure 1 shows the ADC, APEXw, APTw, R_2, and R_1 maps in three representative rats at 1 and 4 h after MCAO onset. The lesion size on ADC maps remained almost constant except in Rat #1, where a slight increase with time was observed. The APEXw maps showed hyperintensity in the lesion area as reported in our earlier study (6). In most rats, the APEXw contrast decreased with time as can be seen in Figure 1. The APTw maps showed darkening in the lesion area, consistent with earlier observations (1,2,6,26). No clear contrast between the lesion and neighboring tissues was present in the R_2 maps at 1-h postocclusion as commonly observed (2,6). At 4 h, the R_2 values in the lesion area slightly decreased, although lesion boundary still cannot be clearly defined. In rats #1 and #3, R_1 values were clearly reduced in the lesion areas even at 1 h. The reduction progressed with time and became more evident in all three rats at 4 h.

Representative proton MR spectra on the contralateral and lesion sides are shown in Figure 2. The lactate peak

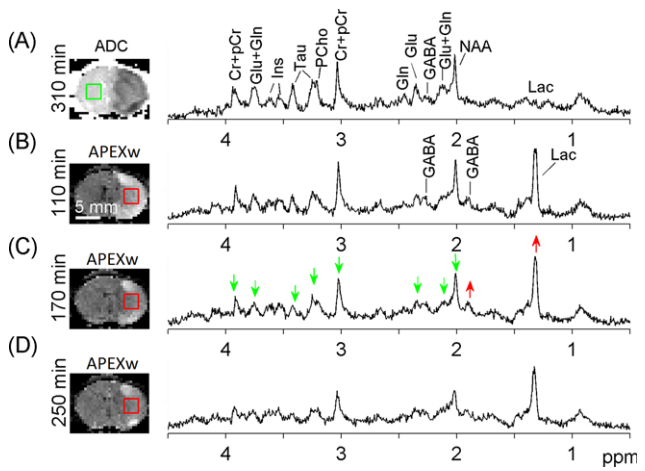

FIG. 2. Localized ^{1}H MR spectra on the contralateral (a) and lesion (b–d) ROIs in a representative rat. The time for each measurement relative to the MCAO onset is given, and the ADC (a) and APEXw maps (b–d) measured at similar time points are displayed together with the voxel locations for the spectroscopy measurements. Green and red arrows indicate metabolite peaks that were reduced and increased compared to the contralateral side, respectively. No smoothing was applied to the spectra. [Color figure can be viewed in the online issue, which is available at wileyonlinelibrary.com.]

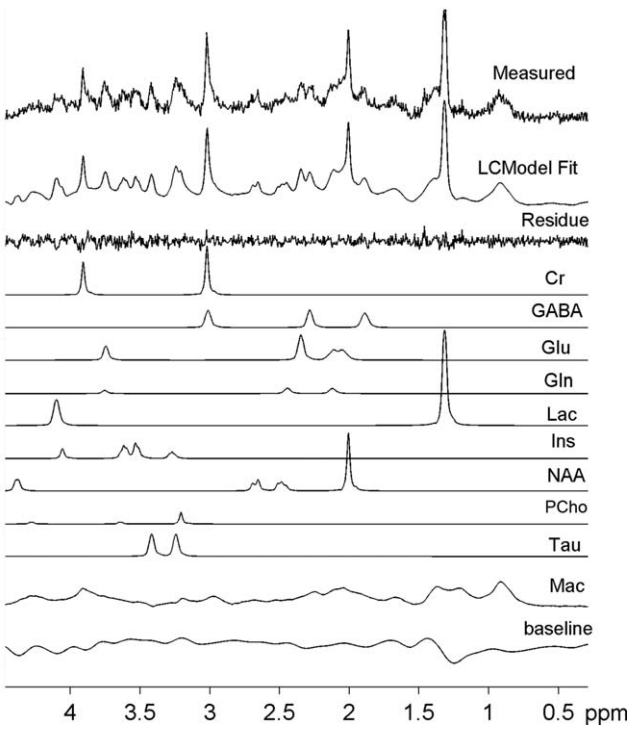

FIG. 3. A representative example of LCModel result. The difference between the measured spectrum and the LCModel fit is displayed as the residue trace. Individual contributions from the 10 model spectra are also displayed as well as an estimated cubic spline baseline.

at 1.3 ppm was dominant on the lesion side (b–d), whereas it was very small on the contralateral side (a). The GABA peaks at ~1.9 and ~2.3 ppm were also more prominent on the lesion side compared to the contralateral side (red upward arrows). Furthermore, the NAA, Tau, and tCr peaks clearly decreased with time on the lesion side (green downward arrows). The LCModel model approach resulted in highly reproducible fitting results for all spectra. The simulated model spectra and a typical example of LCModel fitting results are shown in Figure 3. Except for Lac on the contralateral side and Gln on both hemispheres, the other seven metabolites can be quantified with CRLB less than 25% in most cases.

Quantitative Time-Dependent Analysis of Normal and Ischemic Regions

Time-dependent changes of ROI-averaged imaging data are plotted in Figure 4. ADC, APEXw, APTw, R_2, and R_1 values did not change significantly with time on the contralateral side (one-way ANOVA; $P>0.05$). On the lesion side, ADC, APTw, and R_1 were reduced, whereas APEXw increased compared to the contralateral region. Contrast between normal and ischemic tissues is much higher in APEXw ($3.1\pm1.1\%$ of M_0 during the first period than APTw ($1.8\pm0.5\%$ of M_0 in the first hour), demonstrating that APEXw has much higher ($P=0.008$; two-sample t-test) detectability of ischemic regions as shown in Figure 1. Over the 4.5-h time period, ADC decreased as well as R_1, R_2, and APEXw, whereas APTw remained similar. Interestingly, R_2 on the lesion side was slightly higher than on the contralateral side before 110 min (paired t-test, $P=1.6\times10^{-4}$). The reduction of APEXw slowed down after ~3 h.

Group-average metabolite concentrations are displayed in Figure 5. Concentrations of lactate and GABA were higher on the lesion side compared with the contralateral side and did not change with time. In contrast, concentrations of Glu and Tau were significantly lower on the

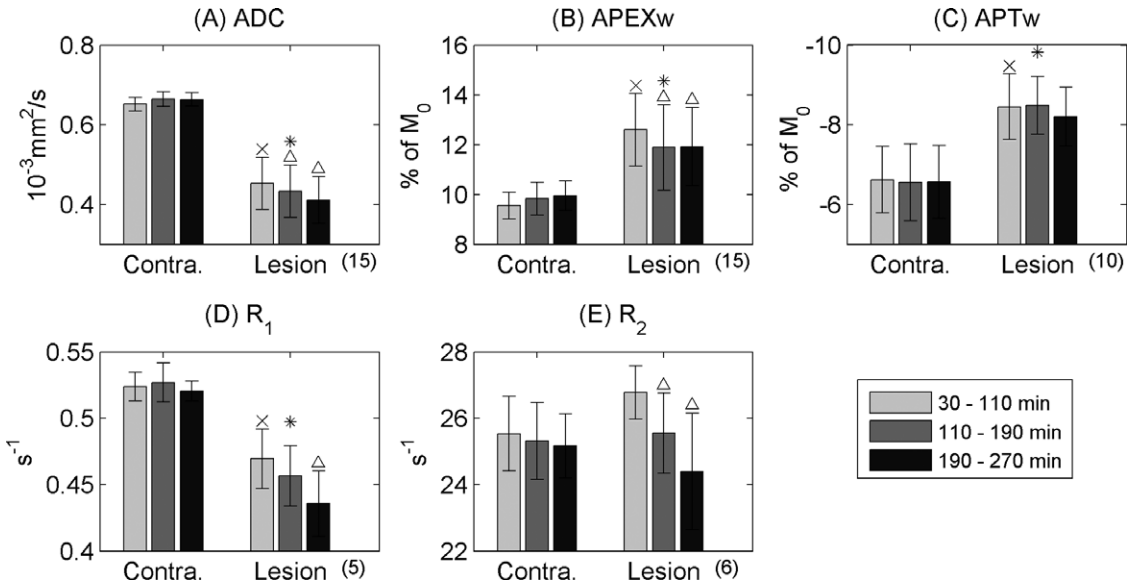

FIG. 4. Time dependence of group-averaged ADC (a), APEXw (b), APTw (c), R_1 (d), and R_2 (e). An "x" mark indicates a significant difference of the first ischemic data point compared to the contralateral side (paired t-test; $P<0.05$ after Bonferroni correction). A "*" sign denotes significant difference between the means of the lesion and contralateral sides (paired t-test; $P<0.05$ after Bonferroni correction). A "Δ" mark denotes $P<0.05$ for a posteriori paired t-test when comparing the last two data points with the first data point when ANOVA reveals significant temporal dependence. Error bars denote standard deviations. The numbers in the parentheses below the x axes are the numbers of animals used for each result.

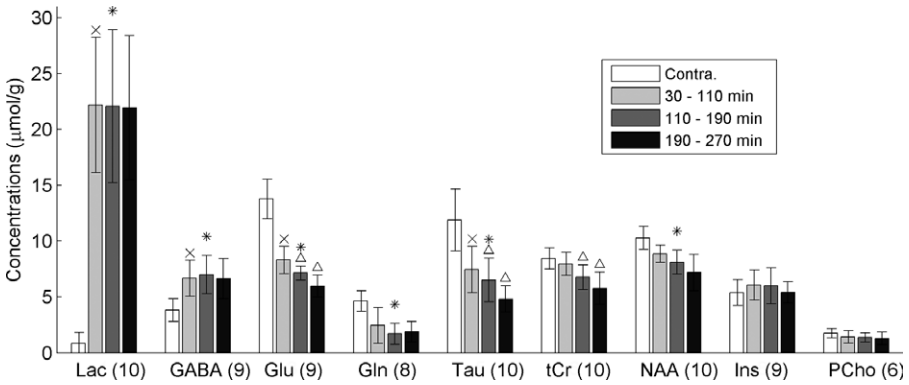

FIG. 5. Group-averaged metabolite concentrations as quantified by LCModel. The meanings of the "x," "*," and "Δ" marks are the same as in Figure 4. Error bars denote standard deviations. Only data meeting our CRLB criteria were included. The numbers next to each metabolite label are the numbers of animals used for each result.

lesion side compared with the contralateral side at the 30–110 min after MACO (see "x" marks), and the concentrations of tCr, Glu, NAA (although not statistically significant), and Tau decreased with time (see "Δ" marks in Fig. 5). For Ins and PCho concentrations, no significant difference was found between the two hemispheres. The observed concentration changes are in general agreement with the literature (see Discussion for details).

Theoretical Results of APEXw and APTw

Figure 6 shows the theoretical curves of APTw and APEXw versus k, p_b, R_2, and R_1. The APEXw versus k curve (red curve in Fig. 6a) exhibits a peak at $k \sim 3000$ s^{-1}, which is approximately equal to the expected peak of R_{ex} versus k (3142 s^{-1}). Ischemia increases in vivo APEXw, indicating that the dominant contributing exchangeable protons have $k > \sim 3000$ s^{-1}, and the APEXw are closer to the peak at lower pH (see red arrow). When the labile proton frequency $\delta = 3.5$ ppm, APTw is maximal at k of ~ 400 s^{-1} (thick black curve in Fig. 6a), and amide protons with exchange rates less than ~ 400 s^{-1} produce a reduction of APTw when k (i.e., pH) decreases (see black arrow). The contribution of amine protons with $\delta = 3.0$ ppm to the APTw signal is significant and the peak shifts to a higher exchange rate of 1260 s^{-1} (thin black curve). Therefore, for amine protons with exchange rates much higher than 1260 s^{-1}, the

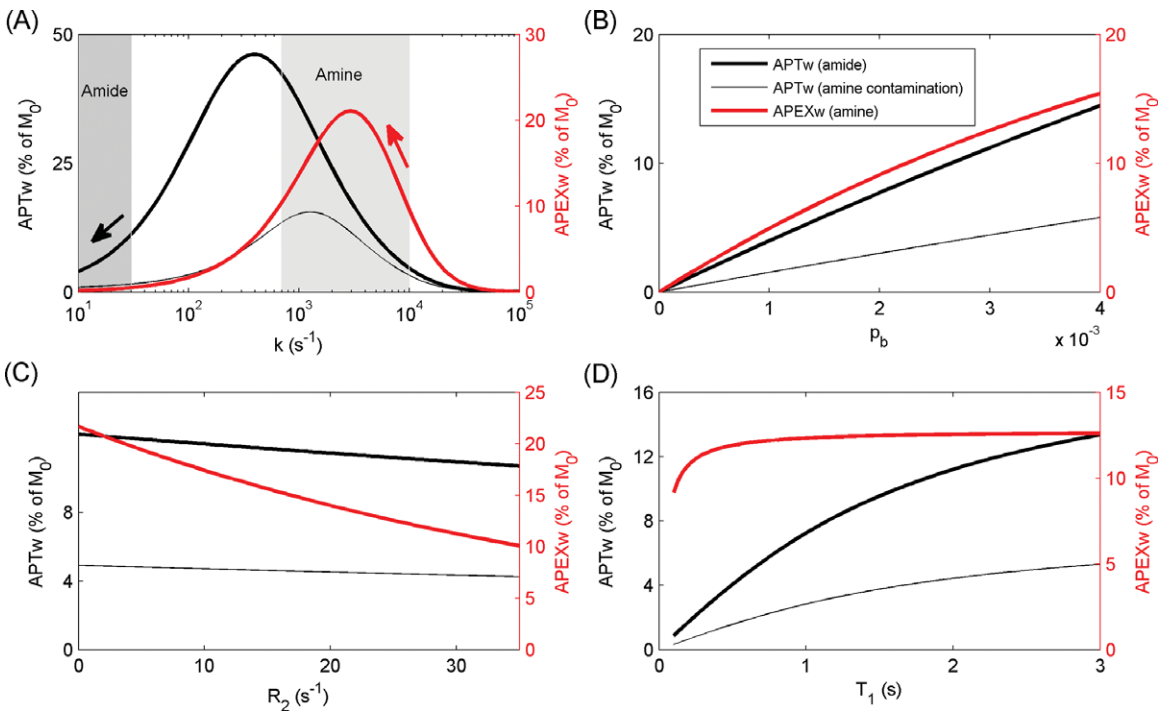

FIG. 6. Theoretical analyses of the dependences of APEXw and APTw on exchange rate (k) (a), labile proton concentration (b), R_2 (c), and T_1 (d). The labile protons were assumed to have a resonance frequency of 3.0 ppm (amine) or 3.5 ppm downfield from water (amide). In all panels, the parameter values were $k = 8000$ s^{-1} for amine and $k = 30$ s^{-1} for amide, $p_b = 0.003$, $R_2 = 25$ s^{-1}, and $T_1 = 2$ s, except for the parameter on the x axis. The shaded regions denote the ranges of the experimental amide (10–30 s^{-1}) and amine proton exchange rates (700–10000 s^{-1}) (1,31). The red and black arrows denote the directions of APEXw and APTw changes, respectively, with decreasing pH under ischemia. APEXw refers to MTR_{asym} at 2.5 ppm and −2.5 ppm measured with the APEX-weighted SL pulse sequence, and APTw refers to MTR_{asym} at 3.5 ppm and −3.5 ppm measured with the APT-weighted CEST technique. The thin gray curves indicate the contribution of APEX effect to APTw signals.

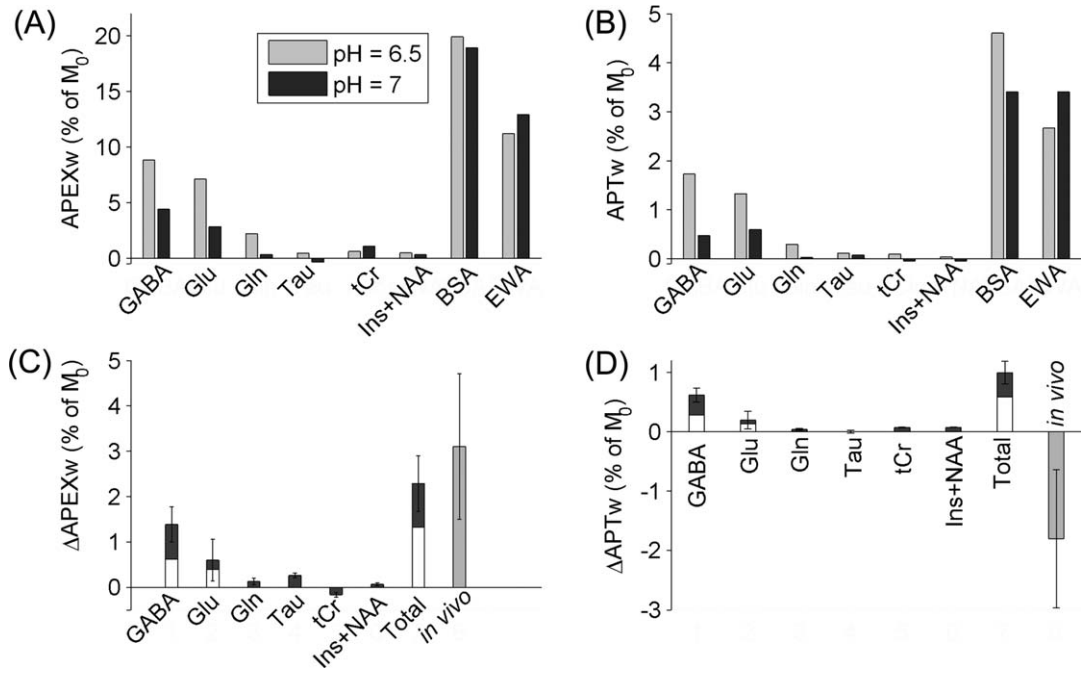

FIG. 7. Phantom data and estimated contribution of metabolites to in vivo APEXw and APTw changes. **a**: APEXw and **b**: APTw in metabolite and protein phantoms at pH of 7 and 6.5. The concentrations of the GABA, Glu, Gln, and Tau solutions are 20 mM, whereas the tCr solution contains 10 mM of Cr and PCr each, and the Ins+NAA mixture solution contains 10 mM of Ins and NAA each. The concentrations of the BSA and EWA phantoms are 8% by weight. All measurements were performed at 37°C at 9.4 T. **c:** Expected APEXw and **d:** APTw changes (ΔAPEXw and ΔAPTw) due to changes in pH (from 7 to 6.5) and in metabolite concentrations. Metabolite concentrations were obtained from in vivo data shown in Figure 5 (left two bars in each group), and their standard deviations were propagated to generate the errors shown here. The black and gray bars on the right denote the sum of contributions from metabolites (total) and the in vivo contrast, respectively. When our Glu and GABA concentrations for the contralateral side were scaled to match values from literatures (33–36), their contributions are shown as white bars. APEXw refers to MTR_{asym} at 2.5 ppm and −2.5 ppm measured with the APEX-weighted SL pulse sequence, and APTw refers to MTR_{asym} at 3.5 ppm and −3.5 ppm measured with the APT-weighted CEST technique.

decreased exchange rate in ischemic conditions may result in an increase of the APTw signal.

APEXw and APTw signals increase almost linearly with labile proton concentration (Fig. 6b). APEXw is more sensitive to R_2, but less sensitive to R_1 than APTw (Fig. 6c,d). Because $\theta \approx 27^\circ$ and $\sim 2.6^\circ$ in Eq. [2] for APEXw and APTw measurements, respectively, the effect of R_2 is quite significant on APEXw, but not on APTw signal (27). When R_2 decreases from 27 to 24 s^{-1}, APEXw increases by 0.8% of M_0 and the APTw signal only decreases by 0.05% of M_0 with δ=3.0 ppm and by 0.15% with δ=3.5 ppm. Within the T_1 range (0.9–2.2 s) encountered in our phantom and animal experiments, the dependence of APEXw on T_1 is negligibly small, whereas the APTw dependence on T_1 is close to linear (Fig. 6d). The deviation from a linear dependence is partly due to the relatively short saturation pulse used in our calculations. With saturation pulse duration of 3 s, the water magnetization does not have enough time to relax toward the steady state due to long T_1 values, thus reducing the APTw signal.

APEXw and APTw of pH-Dependent Phantoms

Both the APEXw and the APTw signals are sensitive to pH and labile proton concentrations. Amine protons are present in Cr, PCr, Glu, Gln, GABA, Tau, and the side-chains of lysine and arginine residues in proteins and peptides, whereas amide protons are present in NAA, Gln, and the backbones of proteins and peptides. To better understand the sources of the observed APEXw and APTw signal changes induced by ischemia, APEXw and APTw in phantom samples were measured at pH of 7.0 and 6.5 (Fig. 7a,b). When the pH in ischemic regions was estimated from the measured Lac concentration from the formula: pH = -0.0335[Lac] + 6.83 with [Lac] in units of μmol/g and valid for [Lac] between 5 and 30 μmol/g (28), pH=6.1±0.2 using our measured [Lac] of 22.2±6.0 μmol/g at the first time point (similar at the other two time points since no significant [Lac] change with time). In earlier studies, pH values in the range of 6.1–6.8 have been reported in ischemic brain regions (1,28–30). The pH of 6.5 in our phantoms likely lies in the middle of the possible pH range of tissues under ischemic conditions.

The two protein solutions had the largest APEXw values, but small (<7%) pH-induced relative changes at opposite directions. GABA and Glu solutions had the largest APEXw values among the metabolite phantoms and showed a large increase at pH=6.5 compared to pH=7, consistent with the slowdown of CE at a lower pH with $k > \omega_1 = 3142 s^{-1}$ (see also red arrow in Fig. 6a). For Gln, the APEXw was negligible (=0.3%) at pH=7 but

increased to 2.2% at pH=6.5, suggesting a higher exchange rate than GABA and Glu. The APEXw of the Tau solution was negligible (<0.5%) at both pH values, suggesting the exchange rates were too fast to be detected. The Ins+NAA mixture solution without containing any amine protons had negligible APEXw (<0.5%) at both pH values. As the tCr solutions containing guanidine protons with relatively low exchange rates (700–1200 s^{-1} (31)), its APEXw signal is small compared to GABA and Glu, and its pH dependence is opposite to GABA and Glu.

Interestingly, the APTw signal showed a pattern across solution composition and pH similar to APEXw. The two protein samples had the largest APTw values, and their pH dependences were the same as for APEXw. Although no amide protons are present in Glu and GABA, large APTw signals were observed at pH=6.5, indicating the effects of amine proton exchange on the APTw signal. The APTw values in NAA were negligible, despite the presence of amide protons, which might be explained by the fact that the resonance frequencies of the amide protons (3.1 ppm) is away from the 3.5-ppm saturation pulse frequency used in the APT experiment and their exchange rates are small (32). The APTw signals in amine-containing metabolites Tau and tCr were very small, possibly due to their unfavorably fast and slow exchange rates, respectively. Gln contains both fast-exchanging amine protons and slow-exchanging amide protons, and its APTw is negligible at pH=7 but increases at pH=6.5, suggesting negligible contribution from the amide protons at pH=7, while the contributions from amine proton exchange might become important at lower pH. Negligible amide contribution to APTw in Gln is also consistent with the large difference of amide resonance frequency in Gln from the 3.5 ppm saturation pulse frequency (32). Ins contains exchangeable protons from the hydroxyl group and does not contribute any significant APTw signal.

Neurometabolite Contributions to the In Vivo APT and APEX Contrast

Based on the phantom and theoretical results and assuming a pH of 6.5 in the ischemic region, the relative contributions of the different metabolites to the observed APEXw and APTw contrasts (ΔAPEXw and ΔAPTw) can be estimated as

$$\Delta S = f_{T1} f_{T2} (C_{\text{ischemia}} S_{6.5} - C_{\text{control}} S_{7.0})/20 \qquad [4]$$

where S is the measured APEXw or APTw value in the phantoms with 20 mM concentrations; the subscript denotes the pH; C_{ischemia} and C_{control} denote the metabolite concentrations (mM) on the lesion and contralateral sides, respectively; and f_{T1} and f_{T2} are correction terms for the T_1 and T_2 differences between phantoms and rats, respectively. The contributions of the metabolites to the observed ΔAPEXw and ΔAPTw during the 30–110 min period are given in Figure 7c,d, respectively. The f_{T1} and f_{T2} factors were estimated based on the theoretical results in Figure 6. They are almost constant between the two δ values for APTw and vary slightly between the lesion and contralateral sides: for APEXw, f_{T1}=1.01 and f_{T2}=0.66–0.69 and for APTw, f_{T1}=1.29–1.36 and f_{T2}=0.92–0.93. The estimated contributions of neurometabolite changes induced by ischemia to ΔAPEXw are of similar magnitude as the measured in vivo ΔAPEXw. The GABA and Glu concentrations averaged over the values in cortex and striatum from literature (33–36) are lower than our values on the nonlesion hemisphere (1.7 μmol/g vs. 3.8 μmol/g for GABA and 9.1 μmol/g vs. 13.8 μmol/g for Glu). In case of overestimates of our Glu and GABA concentrations, their contributions to the ΔAPEXw and ΔAPTw contrasts would be reduced, and the corrected values by multiplying by their ratios are given by the overlaying white bars in Figure 7c,d. Even in this case, GABA and Glu are still major contributors to ΔAPEXw. The estimated contribution of GABA is maximal among the metabolites for both ΔAPEXw and ΔAPTw. The large GABA contribution is due both to the increased GABA concentration and pH reduction in the ischemic region. The sign of the metabolite ΔAPTw is opposite to the observed in vivo ΔAPTw, suggesting that the true ΔAPTw due to amide-proton exchanges is larger than the observed in vivo value of 1.8±1.2%.

DISCUSSION

Sensitivities of the APEX and APT for Stroke Imaging

Several CE-sensitive MR techniques have been investigated for early detection of ischemic brain tissues in rat MCAO models, including SL and CEST techniques. With adiabatic SL pulses (effectively a mixture of on- and off-resonance conditions), $R_{1\rho}$ in the ischemic region is lower than in the nonlesion tissues and the difference increased from ~9% to ~13% between 60 and 150 min after the onset of MCAO with a mean SL pulse power of 2550 Hz at 4.7 T (28). Similar $R_{1\rho}$ contrast was observed under on-resonance condition using a constant SL pulse of 3.4 kHz B_1 field (37). The image contrast is approximately equal to $\tau \Delta R_{1\rho} \exp(-\tau \cdot \bar{R}_{1\rho})$, where τ is the SL time, $\bar{R}_{1\rho}$ is the mean $R_{1\rho}$ value in ischemic and nonlesion tissues and $\Delta R_{1\rho}$ is their difference. The contrast is maximized when $\bar{R}_{1\rho}\,\tau = 1$ and is equal to $\Delta R_{1\rho}/\bar{R}_{1\rho}\,e^{-1}$. In Ref. 28, $\bar{R}_{1\rho}$ = 11.9 s^{-1} and $\Delta R_{1\rho}$ = 1.1 s^{-1} at 60 min post-MCAO, resulting in a maximal image contrast between the ischemic and nonlesion tissues of 3.3% of M_0. In this study, the off-resonance SL-based APEX technique has a contrast of 3.1±1.1% of M_0 during the first hour, which is similar to on-resonance SL contrasts, while its RF power is much smaller than in the earlier on-resonance and adiabatic SL studies (0.5 kHz vs. 2.5–3.4 kHz).

Earlier APT studies have reported lesion contrasts of 1.8–2.1% in rat MCAO models at 4.7 and 9.4 T (1,26,38). In this study, the APTw contrast is 1.8±1.2% (mean±STD) of M_0 during the first period, consistent with the earlier studies. The APEXw contrast of 3.1±1.1% of M_0 during the first period corresponds to a large sensitivity increase compared to the APTw contrast. The positive contrast of the APEXw signal in the ischemic regions is preferable over the negative APTw contrast for stroke lesion detection, because lesions can be more easily distinguished from dark background in positive contrast images. Furthermore, the APEXw signal is much less contaminated by the MT asymmetry from

Table 1
Comparison of Metabolite Concentrations Measured in Nonischemic Brain In Vivo by MRS in Different Studies[a]

		Lac	GABA	tCr	Glu	NAA	Tau	Gln	Ins	PCho
Striatum (33,35,36)		1.3–1.8	1.1–2.3	5.8–8.5	7.9–8.6	7.1–7.7	1.9–10.9	1.7–3.7	3.7–6.3	1.0–1.9
Cortex (34–36)		1–1.5	0.8–2.2	5.4–8.5	8.5–11	6.9–10	3.3–8.0	2.3–3.4	3–6.1	0.6–1.0
This study	Contra	0.8±1.0	3.8±1.0	8.4±0.9	13.8±1.8	10.3±1.0	11.9±2.8	4.6±0.9	5.4±1.2	1.8±0.4
	Lesion	22.2±6.0	6.7±1.6	7.9±1.1	8.3±1.2	8.9±0.7	7.5±2.0	2.5±1.5	6.1±1.3	1.4±0.5

[a]The voxels in our study cover both striatum and lower parietal cortex. The values in Ref. 35 are for rats of 4 weeks old. All concentrations are in units of μmol/g. The errors are standard deviations across animals. The data on the lesion side were measured during the first period of 30–110 min after MCAO.

semisolid macromolecules and nuclear Overhauser effects compared to the APTw contrast, because the MT asymmetry and nuclear Overhauser effects are typically maximized with long and weak saturation pulses, and their effects should be minimal with a short SL pulse of 150 ms (26).

Comparison with Spectroscopy Literature

Increase of Lac concentration following brain ischemia is well established (39–47). Within the first few hours after permanent MCAO onset, the Lac concentration either gradually increased or quickly reached a plateau within the first hour (40,42,43,48,49). Brain ischemia was found to stimulate GABA synthesis and inhibit GABA breakdown, resulting in an increase of GABA concentration (39,50,51), consistent with our finding.

We observed reduction of concentrations of NAA and total creatine (tCr) in the lesion area within ~4.5 h after MCAO onset. Reduction in NAA concentration has been widely reported in rat and human brains under ischemic conditions (40–43,52–59). A 30–70% decrease of total creatine concentration within a few hours of permanent MCAO onset has been reported in the literature, comparable to our result (35±15% at ~4 h) (42,45,46). MCAO also resulted in reductions of Glu and Tau concentrations, consistent with earlier findings (50,60–62). The Gln concentration was also reduced in our study, which is consistent with earlier measurements performed 24 or 36 h after onset of permanent MCAO (47,62). However, (60) and (61) observed 70–100% increase of Gln concentration at 3–8 h after ischemia onset in rats subjected to 30 min transient ischemia. Increased glutamine after reperfusion may be explained by the recovered function of Glu to Gln conversion in glial cells.

It is well known that water content increases in ischemic brain tissues (18,63,64), which will impact quantification of metabolite concentrations. Striatum water contents of 77 and 79% have been reported in the contralateral and ipsilateral hemisphere, respectively, 2 h 15 min after MCAO in rats (18). In Ref. 63, water content in ischemic tissue gradually increased with time and was 2.3% (absolute change) higher than control animals at 4 h after MCAO. We assumed constant water content of 79% when calculating the metabolite concentrations on the lesion side, which would slightly under-estimate the concentrations at later time points compared to the earlier time points. However, we note that the observed gradual concentration reduction of Cr, Glu, and Tau were not solely due to the increase of water content with time since significant reduction with time were still observed even when assuming a linear increase of water content from 77% after MCAO onset at 1% per hour.

Table 1 summarizes metabolite concentrations and compares them with literature values measured also in rats with localized spectroscopy. As the STEAM voxels mostly covered the striatum and lower parietal cortex, only literature values for the striatum and the cortex are included in the table. Most of our concentration values lie within the range reported in the literature except for Glu and GABA. Our values for Glu and GABA appear higher (25±16% for Glu and 65±43% for GABA) than the upper limits of the earlier in vivo studies (33–36), although similar Glu and GABA concentrations as ours have been reported in MRS and liquid chromatography studies on extracted brain tissues (50,65).

Signal Sources of the APEXw Contrast

According to Eq. [3], under our experimental conditions the APEXw signal is most sensitive to labile protons with chemical shift of 2.5 ppm from water and with an exchange rate of 3140 s^{-1}. The amine protons have chemical shifts in the range of 2–3 ppm and have a range of exchange rates (~700–10,000 s^{-1}) under physiological conditions (pH=7.0 and temperature=37°C) (31,66). Thus, the experimental conditions for the APEXw measurement were well tuned to the fast amine proton exchange processes.

In vivo APEXw value was 9.5±0.5% of M_0 on the contralateral side. Based on our phantom study, GABA and Glu would contribute ~1.1% and ~2.5% of M_0 to APEXw, respectively, at pH=7.0 and at concentrations same as measured on the nonlesion hemisphere (~4.8 and 17.5 mM, respectively, assuming metabolites are all dissolved in water, a brain density of 1 g/ml, and a brain water content of 79%), although it is likely that the in vivo APEXw due to metabolites are different from the values in the phantoms at the same pH due to the dependence of CE rate on catalyzing-ion concentrations (31). Nevertheless, the small estimated GABA and Glu contributions indicate that the in vivo APEXw signal cannot be explained solely by contributions from metabolites, meaning proteins likely have large contributions to the observed in vivo APEXw.

Although the neurometabolites in the brain have small contributions to the APEXw signal relative to proteins at normal tissues, their relative contributions to ΔAPEXw (the APEXw contrast of ischemia) might be much larger (see Fig. 7c). The BSA and EWA phantoms show weak

and opposite dependences on pH (Fig. 7a), suggesting that the protein contribution to APEXw might not be very sensitive to pH, so that the relative protein contributions to the ΔAPEXw is much smaller than to APEXw. The weak pH dependence of APEXw can arise in case of a broad distribution of amine proton exchange rates in proteins (67). We note that the initial R_2 increase of ~1 s^{-1} in the ischemia regions cannot explain the observed initial positive ΔAPEXw either. From the theoretical analysis, the initial R_2 increase would decrease APEXw by 0.4% of M_0 (Fig. 6c), opposite to and much smaller than the observed positive ΔAPEXw of 3.1% of M_0.

Recently, based on CEST studies attempting to image glutamate concentrations (GluCEST) in the brain (23), the contrast between stroke and nonlesion rat brain regions was minimal at 1 h after MCAO onset and increased between 1 and 5 h of MCAO onset. As the GluCEST has a GABA contribution of only ~20% of the Glu contribution under normal physiological conditions, Cai et al. attributed the increase of the positive CEST contrast to an elevated glutamate CEST signal in the ischemic tissues because of lower pH (23). Despite differences in saturation pulse parameters ($\gamma B_1/2\pi$=155 Hz, duration=1 s, offset=3.0 ppm vs. 500 Hz, 0.15 s and 2.5 ppm in our studies), the saturation pulse lied within the sensitive spectral window of the amine protons, thus CEST effects due to APEX should be present. However, findings of Ref. 23 are quite different from our APEX data in two folds. (1) The different temporal characteristics may be explained by variations of MCAO models. In our study, the lactate concentration increased rapidly following MCAO and remained constant over time, similar to some earlier studies (42,48). However, other studies have observed interanimal variations of the evolution patterns including a gradual increase of lactate concentration within the first few hours of MCAO in some animals (40,43). (2) In our case, the GABA contribution to ΔAPEXw is larger than the Glu contribution due to increased GABA concentration and decreased Glu concentration, in addition to the rapid elevation of lactate content in the first hour. Thus, to interpret the sources of CE-sensitive ischemic contrast, measurements of metabolite concentrations should be necessary.

A gradual reduction of ΔAPEXw with time was observed (~0.7 % of M_0 in 3 h) (Figs. 1 and 4b), in contrast to a relatively stable ΔAPTw. During rat MCAO, a decrease of on-resonance $R_1\rho$ (increase of $T_1\rho$) over time has been reported (37), which may be able to indicate the onset time of ischemia (5). Further study is necessary to investigate whether the decrease of APEXw signal and on-resonance $R_1\rho$ has similar origins. In our case, the change of ΔAPEXw can be mainly attributed to the reduction of Glu and possibly protein concentrations, as Lac and GABA concentrations were nearly constant during the experiment. Constant Lac concentration suggests a constant pH because of the linear relationship between them (28), although dissociation between dynamically changing pH and Lac concentration has been observed during ischemia (49,68). Therefore, the pH was most likely constant during our experiments. A reduction of Glu concentration by 2.9 mM was observed in our spectroscopic study during the experiments. According to the phantom results at pH=6.5 with consideration of different R_2, this would result in a reduction of in vivo APEXw by ~0.7% of M_0. A possible decrease in the concentration of proteins may also contribute to the reduction of ΔAPEXw over time; an increase of water content from 77 to 79% would result in the reduction in the concentration of other chemical components from 23 to 21%, which corresponds to 11% $(= 1 - 21 \times 77/(79 \times 23))$ reduction in their ratio to water. Due to the large protein contribution to the baseline APEXw signal, an 11% reduction in protein concentration can contribute 0.5–1% of M_0 to the reduction in APEXw. The reduction of APEXw appeared to slow down after the second time point (Fig. 4b). One possible explanation is the effect of R_2 change on APEXw. In our MCAO study, R_2 decreased from 26.8±0.8 s^{-1} to 24.4±1.8 s^{-1} between the first and the third time points (Fig. 4e), and our theoretical results suggest that this can result in a significant increase of APEXw (Fig. 6c). However, we note that the measured transverse relaxation rate contains the exchange contribution R_{ex}, which should not be included in the R_2 in Eq. [2] and Figure 6c. The reduction of the intrinsic R_2 excluding the exchange contribution might be slightly smaller than observed in Figure 4e.

Signal Sources of the APTw Contrast

Ability of a CE technique for measuring one type of labile proton is closely related to its exchange rate (6,8). For example, for amine of Glu at 3 ppm with an exchange rate of ≥5000 s^{-1}, the peak of R_{ex} versus offset frequency is very broad, and the variation of R_{ex} is less than 7% within the Ω=2.5–3.5 ppm range (Eq. [3]). Therefore, the fast APEX will likely contaminate the measurement of APTw at 3.5 ppm. Our phantom and theoretical results suggest that the observed negative ΔAPTw in ischemic brain regions is a combined effect of at least two contributions: the faster APEX in GABA, Glu, proteins, and peptides ($\Delta APTw_{amine}$), and the slower amide-proton transfer ($\Delta APTw_{amide}$). Due to the much faster rate of the APEX, GABA and Glu have positive $\Delta APTw_{amine}$ (Fig. 7d) with reduced pH. Therefore, the contribution of APEX increases the positive baseline APTw signal and reduces the measured negative in vivo ΔAPTw.

In addition to metabolites, APEX effect from proteins also can affect APTw. In the protein phantoms, both amine and amide protons are present, and the contamination of the APT signal will be mainly due to the amine group of the lysine residues with an exchange rate close to 4000 s^{-1} (31). The different pH dependence of the APTw signals for BSA and EWA phantoms can be attributed to the competition between $\Delta APTw_{amine}$ and $\Delta APTw_{amide}$. In BSA which has a high lysine content (12.82% weight fraction) (69), $\Delta APTw_{amine}$ may be dominant over $\Delta APTw_{amide}$, therefore a positive ΔAPTw is observed for a pH change from 7 to 6.5. In EWA, $\Delta APTw_{amide}$ may be larger than $\Delta APTw_{amine}$; therefore, a negative change of APTw signal is observed. In ovalbumin, the main protein found in EWA, the lysine content

is only 5.0% molar fraction (70) in support of our observation.

The APTw did not significantly change with time during the experiment. To explain the APTw time course, we first note that pH in the lesion regions remained constant, because no lactate concentration change was observed. Besides its strong dependence on pH, the APT signal is proportional to the ratio of labile proton to water concentrations. As discussed earlier, an increase of water content would result in 10% reduction in amine and amide concentrations and would decrease $\Delta APTw_{amine}$ and $\Delta APTw_{amide}$ during the first few hours after MCAO onset. However, the decreases in ΔAPT_{amine} and ΔAPT_{amide} due to concentration changes might be offset by lengthening T_1 [by 8% between 1 and 4 h (Fig. 3d)] which increases the APTw signal, resulting in almost constant APT time course in our study.

Limitations of Signal Source Study

The APEXw and APTw contributions from neurometabolite estimated based on our phosphate-buffered saline solutions and spectroscopy results are likely different from their true contributions in the brain. First, the CE rates of APEX and APT processes depend not only on temperature and pH but also on the concentrations of exchange catalysts other than proton and hydroxide. The concentrations of those exchange catalysts are likely different between the brain and phosphate-buffered saline solution used in our phantoms. Second, there are a wide variety of proteins in the brain, and they may have very different amino acid compositions than BSA and EWA. They also have different degree of cross-link, folding, and only some of the proteins in the brain are in mobile form and the others form semisolids with very short T_2 values. The amine protons associated with those immobile proteins have very broad line width and thus their contributions to the APEXw and APTw signal could be greatly reduced. Third, semisolid MT effect and nuclear Overhauser effects (26) are very small in phantoms. In brain, these effects may significantly reduce the APTw and APEXw amplitudes. Fourth, a pH of 6.5 was used for our low pH phantoms. However, the in vivo pH values in the ischemic tissues are likely different and also spatially heterogeneous and may vary from animal to animal. Last, the Glu and GABA concentrations might be overestimated according to the literature values (33–36). The reason for the discrepancy is unclear. However, even after scaling our Glu and GABA concentrations to match the mean literature values, the neurometabolite contributions are still significant relative to the observed in vivo ΔAPEXw and ΔAPTw and the relative contribution of GABA and Glu to ΔAPEXw remains similar (See Fig. 7c,d). Due to the above uncertainties, the results from the phantom study should only be applied in a qualitative manner to understand the in vivo sources of the APTw and APEXw signals.

CONCLUSIONS

The APEX can be imaged using the off-resonance SL or CEST techniques, and the APEXw signal has a higher sensitivity than APTw for detecting ischemic brain tissue. At normal pH (pH=7.0), mobile protein/peptide has the largest contribution to the APEX signal. At reduced pH under ischemic conditions, contributions from neurotransmitters GABA and Glu increase and might become important sources of the observed initial hyperintensity in ischemic regions in the APEXw maps. The APTw signal has contributions from the well-known amide-proton exchange as well as from the faster APEX; the latter increases baseline APTw signal and may reduce the APTw contrast for ischemic tissues. Such contamination is dependent on the irradiation pulse parameters and may also be dependent on the B_0 field strength. In contrast to a constant APTw signal time course, a reduction of the APEXw signal with time is observed, suggesting a high sensitivity of the APEXw contrast to biomolecular concentration changes. It should be emphasized that when neuropathological conditions change pH, metabolite, and protein concentrations; physiological interpretation of APTw and APEXw contrasts is complex and requires caution.

ACKNOWLEDGMENTS

The authors thank Kristy Hendrich for maintaining the 9.4 T MRI system and Hunter Mehrens for proofreading our manuscript.

APPENDIX

In this appendix, the implementation of model spectra simulation by the density matrix formalism within MATLAB is described. When no RF pulse and magnetic field gradient is applied, the Hamiltonian for a metabolite is described in the rotating frame at the RF pulse frequency by

$$H_m = 2\pi \sum_{i,j} J_{ij} \vec{I}_i \cdot \vec{I}_j - 2\pi \sum_i K_i I_{i,z}, \quad [A1]$$

where $\vec{I}_l$ and $\vec{I}_j$ stand for the spin operator of the *i*th and *j*th observable (i.e., nonexchangeable) protons, respectively, K_i is the difference of its resonance frequency and the RF pulse frequency due to chemical shift, J_{ij} is the J-coupling constants between spins *i* and *j*. The values of K_i and J_{ij} are taken from Ref. 71. During the experiment, field gradients are applied for voxel localization and for dephasing coherences other than those involved in the stimulated echo generation. When a gradient is applied, the following term should be added to the Hamiltonian in Eq. [A1]:

$$H_g = -2\pi\Lambda \sum_i I_{i.z}, \quad [A2]$$

where Λ is the spatial dependent frequency shift due to the gradient field. Furthermore, when an RF pulse is applied, another term should be added to the Hamiltonian:

$$H_{rf} = -B_1\gamma \sum_i \left(I_{x,i}\cos\theta + I_{y,i}\sin\theta\right), \quad [A3]$$

where θ is the angle of the B_1 field in the rotating frame, and γ is the gyromagnetic ratio of protons. The shaped RF pulses each consist of 256 segments, with constant

H_{rf} during each segment. The evolution of the density matrix (σ) under a constant Hamiltonian is

$$\sigma(t_i) = \exp(-iH_i\Delta t_i)\sigma(t_{i-1})\exp(iH_i\Delta t_i), \quad [A4]$$

where H_i is the Hamiltonian from time t_{i-1} to t_i and $\Delta t_i = t_i - t_{i-1}$. The evolution of the density matrix from the initial thermal equilibrium value can thus be calculated for the entire pulse sequence using Eq. [A1–A4] without numerical integration. In our program, all spin operators, the Hamiltonians, and σ are represented by $2^n \times 2^n$ matrices in the Hilbert space formed by the eigenvectors of $I_{i,z}$, where n is the number of observable protons in the metabolite.

The spatial-encoding gradients were not simulated. Their effect is equivalent to shifting the frequencies of the RF pulses which does not affect the shape of the simulated spectrum as long as all resonance frequencies are still within the selective band of the RF pulses. In contrast, the crusher gradients cannot be ignored in order to preserve only the experimentally relevant coherence transfer pathway. Their effects can be simulated by calculating σ evolution with a large set of $\Lambda\tau$ values, where τ is the duration of H_g, and then taking the average over all results (72). Such an approach is time-consuming and complete removal of unwanted coherences is not guaranteed. However, since all unwanted coherences in the resulting σ depend on $\Lambda\tau$ as $\sin(4\pi\Lambda\tau + \varphi)$ for crushing gradients applied during the first and third TE/2 periods, it is sufficient to run the simulation twice at two $\Lambda\tau$ values which differ by 1/4 and sum over the results to remove those coherences. We note that a similar approach was taken in Ref. 73; however, four consecutive $\Lambda\tau$ values were used with steps of 1/4, resulting in doubling of computing time. The crusher gradient during the mixing time (TM) period can be simulated in a similar way. Now the dependence becomes $a_1\sin(4\pi\Lambda\tau + \varphi_1) + a_2\sin(2\pi\Lambda\tau + \varphi_2)$, as both single- and double-quantum coherences are nonzero during the TM period. Therefore, the simulation needs to be run at four $\Lambda\tau$ values with steps of 1/4 to cancel all the oscillating terms. Alternatively, the effect of the crusher gradients during the TM period can be simulated by simply setting the matrix elements in σ that corresponds to single or higher-order quantum coherences to zero (73). Both approaches were tested and found to give identical results. In the final implementation, the second approach was taken to reduce computation time by a factor of 4.

The final NMR signal was calculated as

$$S(l) = \mathrm{trace}\left[\sum_i (I_{x,i} - iI_{y,i})\sigma(\mathrm{TE+TM+}(l-1)/\mathrm{sw})\right] \times \exp\left[-(l-1)R_2^*/\mathrm{sw}\right], \quad [A5]$$

where l=1, 2, 3,..., sw (= 4000 Hz) is the spectral width in the experiment, and the exponential term with R_2^*=25 s^{-1} simulates line broadening (full width at half maximum=8 Hz) due to apparent transverse relaxation. Additional broadening needed to match the real experimental condition was determined during LCModel fitting. The T_1 and T_2 relaxation effects were not simulated because $T_1 >>$ TE+TM and $T_2 >>$ TE in our measurements. For all simulated metabolite and water signals, the signal amplitude $|S(1)|$ is proportional to the number of protons n.

REFERENCES

1. Zhou JY, Payen JF, Wilson DA, Traystman RJ, van Zijl PCM. Using the amide proton signals of intracellular proteins and peptides to detect pH effects in MRI. Nat Med 2003;9:1085–1090.
2. Sun PZ, Zhou JY, Sun WY, Huang J, van Zijl PCM. Detection of the ischemic penumbra using pH-weighted MRI. J Cerebr Blood F Met 2007;27:1129–1136.
3. Grohn OH, Lukkarinen JA, Silvennoinen MJ, Pitkanen A, van Zijl PC, Kauppinen RA. Quantitative magnetic resonance imaging assessment of cerebral ischemia in rat using on-resonance T(1) in the rotating frame. Magn Reson Med 1999;42:268–276.
4. Grohn OHJ, Kettunen MI, Makela HI, Penttonen M, Pitkanen A, Lukkarinen JA, Kauppinen RA. Early detection of irreversible cerebral ischemia in the rat using dispersion of the magnetic resonance imaging relaxation time, T1rho. J Cereb Blood Flow Metab 2000;20:1457–1466.
5. Jokivarsi KT, Hiltunen Y, Grohn H, Tuunanen P, Grohn OHJ, Kauppinen RA. Estimation of the Onset Time of Cerebral Ischemia Using T-1 rho and T-2 MRI in Rats. Stroke 2010;41:2335–2340.
6. Jin T, Wang P, Zong X, Kim SG. Magnetic resonance imaging of the Amine–Proton EXchange (APEX) dependent contrast. Neuroimage 2012;59:1218–1227.
7. Ward KM, Aletras AH, Balaban RS. A new class of contrast agents for MRI based on proton chemical exchange dependent saturation transfer (CEST). J Magn Reson 2000;143:79–87.
8. Jin T, Autio J, Obata T, Kim SG. Spin-locking versus chemical exchange saturation transfer MRI for investigating chemical exchange process between water and labile metabolite protons. Magn Reson Med 2011;65:1448–1460.
9. Kiozumi J, Yoshida Y, Nakazawa T, Ooneda G. Experimental studies of ischemic brain edema: I: a new experimental model of cerebral embolism in rats in which recirculation can be introduced in the ischemic area. The Japanese Journal of Stroke 1986;8:1–8.
10. Kim SG, Hu X, Ugurbil K. Accurate T1 determination from inversion recovery images: application to human brain at 4 Tesla. Magn Reson Med 1994;31:445–449.
11. Sun PZ, Cheung JS, Wang E, Benner T, Sorensen AG. Fast multislice pH-weighted chemical exchange saturation transfer (CEST) MRI with Unevenly segmented RF irradiation. Magn Reson Med 2011;65:588–594.
12. Tkac I, Starcuk Z, Choi IY, Gruetter R. In vivo 1H NMR spectroscopy of rat brain at 1 ms echo time. Magn Reson Med 1999;41:649–656.
13. Gruetter R. Automatic, localized in vivo adjustment of all first- and second-order shim coils. Magn Reson Med 1993;29:804–811.
14. Pfeuffer J, Tkac I, Provencher SW, Gruetter R. Toward an in vivo neurochemical profile: quantification of 18 metabolites in short-echo-time (1)H NMR spectra of the rat brain. J Magn Reson 1999;141:104–120.
15. Provencher SW. Estimation of metabolite concentrations from localized in vivo proton NMR spectra. Magn Reson Med 1993;30:672–679.
16. Lee SP, Silva AC, Ugurbil K, Kim SG. Diffusion-weighted spin-echo fMRI at 9.4 T: microvascular/tissue contribution to BOLD signal changes. Magn Reson Med 1999;42:919–928.
17. Meng Y, Vazquez A, Kim S-G. In vivo arterial blood T2 measurement with arterial spin labeling at 9.4 Tesla. In Proceedings of the 19th Annual Meeting of ISMRM, Montreal, Canada, 2011. p. 372.
18. Barbier EL, Liu L, Grillon E, Payen JF, Lebas JF, Segebarth C, Remy C. Focal brain ischemia in rat: acute changes in brain tissue T1 reflect acute increase in brain tissue water content. NMR Biomed 2005;18:499–506.
19. McIlwain H, Bachelard HS. Biochemistry and the central nervous system. Edinburgh/New York: Churchill Livingstone; 1985. 660 p.
20. Trott O, Palmer AG III. R1rho relaxation outside of the fast-exchange limit. J Magn Reson 2002;154:157–160.
21. Sun PZ, van Zijl PC, Zhou J. Optimization of the irradiation power in chemical exchange dependent saturation transfer experiments. J Magn Reson 2005;175:193–200.
22. Zhou J, Wilson DA, Sun PZ, Klaus JA, Van Zijl PC. Quantitative description of proton exchange processes between water and endogenous and exogenous agents for WEX, CEST, and APT experiments. Magn Reson Med 2004;51:945–952.
23. Cai K, Haris M, Singh A, Kogan F, Greenberg JH, Hariharan H, Detre JA, Reddy R. Magnetic resonance imaging of glutamate. Nat Med 2012;18:302–306.
24. Mcconnell HM. Reaction rates by nuclear magnetic resonance. J Chem Phys 1958;28:430–431.

25. Woessner DE, Zhang S, Merritt ME, Sherry AD. Numerical solution of the Bloch equations provides insights into the optimum design of PARACEST agents for MRI. Magn Reson Med 2005;53:790–799.
26. Jin T, Wang P, Zong X, Kim SG. MR imaging of the amide-proton transfer effect and the pH-insensitive nuclear overhauser effect at 9.4 T. Magn Reson Med 2013;69:760–770.
27. Jin T, Kim SG. Quantitative chemical exchange sensitive MRI using irradiation with toggling inversion preparation. Magn Reson Med 2012;68:1056–1064.
28. Jokivarsi KT, Gröhn HI, Gröhn OH, Kauppinen RA. Proton transfer ratio, lactate, and intracellular pH in acute cerebral ischemia. Magn Reson Med 2007;57:647–653.
29. Sako K, Kobatake K, Yamamoto YL, Diksic M. Correlation of local cerebral blood flow, glucose utilization, and tissue pH following a middle cerebral artery occlusion in the rat. Stroke 1985;16:828–834.
30. Back T, Hoehn-Berlage M, Kohno K, Hossmann KA. Diffusion nuclear magnetic resonance imaging in experimental stroke. Correlation with cerebral metabolites. Stroke 1994;25:494–500.
31. Liepinsh E, Otting G. Proton exchange rates from amino acid side chains—implications for image contrast. Magn Reson Med 1996;35:30–42.
32. Mori S, Eleff SM, Pilatus U, Mori N, van Zijl PC. Proton NMR spectroscopy of solvent-saturable resonances: a new approach to study pH effects in situ. Magn Reson Med 1998;40:36–42.
33. Hong ST, Balla DZ, Shajan G, Choi C, Ugurbil K, Pohmann R. Enhanced neurochemical profile of the rat brain using in vivo (1)H NMR spectroscopy at 16.4 T. Magn Reson Med 2011;65:28–34.
34. Makaryus R, Lee H, Yu M, Zhang S, Smith SD, Rebecchi M, Glass PS, Benveniste H. The metabolomic profile during isoflurane anesthesia differs from propofol anesthesia in the live rodent brain. J Cereb Blood Flow Metab 2011;31:1432–1442.
35. Tkac I, Rao R, Georgieff MK, Gruetter R. Developmental and regional changes in the neurochemical profile of the rat brain determined by in vivo 1H NMR spectroscopy. Magn Reson Med 2003;50:24–32.
36. Xu S, Ji Y, Chen X, Yang Y, Gullapalli RP, Masri R. In vivo high-resolution localized (1) H MR spectroscopy in the awake rat brain at 7 T. Magn Reson Med 2013;69:937–943.
37. Jokivarsi KT, Niskanen JP, Michaeli S, Grohn HI, Garwood M, Kauppinen RA, Grohn OH. Quantitative assessment of water pools by T1rho and T2rho MRI in acute cerebral ischemia of the rat. J Cereb Blood Flow Metab 2009;29:206–216.
38. Sun PZ, Cheung JS, Wang E, Lo EH. Association between pH-weighted endogenous amide proton chemical exchange saturation transfer MRI and tissue lactic acidosis during acute ischemic stroke. J Cereb Blood Flow Metab 2011;31:1743–1750.
39. Peeling J, Wong D, Sutherland GR. Nuclear magnetic resonance study of regional metabolism after forebrain ischemia in rats. Stroke 1989;20:633–640.
40. Norris DG, Hoehn-Berlage M, Dreher W, Kohno K, Busch E, Schmitz B. Characterization of middle cerebral artery occlusion infarct development in the rat using fast nuclear magnetic resonance proton spectroscopic imaging and diffusion-weighted imaging. J Cereb Blood Flow Metab 1998;18:749–757.
41. Gyngell ML, Busch E, Schmitz B, Kohno K, Back T, Hoehn-Berlage M, Hossmann K-A. Evolution of acute focal cerebral ischaemia in rats observed by localized 1H MRS, diffusion-weighted MRI, and electrophysiological monitoring. NMR Biomed 1995;8:206–214.
42. van der Toorn A, Verheul HB, Berkelbach van der Sprenkel JW, Tulleken CA, Nicolay K. Changes in metabolites and tissue water status after focal ischemia in cat brain assessed with localized proton MR spectroscopy. Magn Reson Med 1994;32:685–691.
43. Dreher W, Kuhn B, Gyngell ML, Busch E, Niendorf T, Hossmann KA, Leibfritz D. Temporal and regional changes during focal ischemia in rat brain studied by proton spectroscopic imaging and quantitative diffusion NMR imaging. Magn Reson Med 1998;39:878–888.
44. Igarashi H, Kwee IL, Nakada T, Katayama Y, Terashi A. 1H magnetic resonance spectroscopic imaging of permanent focal cerebral ischemia in rat: longitudinal metabolic changes in ischemic core and rim. Brain Res 2001;907:208–221.
45. Kozlowski P, Buchan AM, Tuor UI, Xue D, Huang ZG, Chaundy KE, Saunders JK. Effect of temperature in focal ischemia of rat brain studied by 31P and 1H spectroscopic imaging. Magn Reson Med 1997;37:346–354.
46. Hesselbarth D, Franke C, Hata R, Brinker G, Hoehn-Berlage M. High resolution MRI and MRS: a feasibility study for the investigation of focal cerebral ischemia in mice. NMR Biomed 1998;11:423–429.
47. van der Zijden JP, van Eijsden P, de Graaf RA, Dijkhuizen RM. 1H/13C MR spectroscopic imaging of regionally specific metabolic alterations after experimental stroke. Brain 2008;131:2209–2219.
48. Higuchi T, Fernandez EJ, Maudsley AA, Shimizu H, Weiner MW, Weinstein PR. Mapping of lactate and *N*-acetyl-L-aspartate predicts infarction during acute focal ischemia: in vivo 1H magnetic resonance spectroscopy in rats. Neurosurgery 1996;38:121–130.
49. Morikawa S, Inubushi T, Takahashi K, Ishii H, Shigemori S. Dissociation between lactate accumulation and acidosis in middle cerebral artery-occluded rats assessed by 31P and 1H NMR metabolic images under a 2-T magnetic field. Magn Reson Imaging 1996;14:1197–1204.
50. Haberg A, Qu H, Saether O, Unsgard G, Haraldseth O, Sonnewald U. Differences in neurotransmitter synthesis and intermediary metabolism between glutamatergic and GABAergic neurons during 4 hours of middle cerebral artery occlusion in the rat: the role of astrocytes in neuronal survival. J Cereb Blood Flow Metab 2001;21:1451–1463.
51. Erecinska M, Nelson D, Wilson DF, Silver IA. Neurotransmitter amino acids in the CNS. I. Regional changes in amino acid levels in rat brain during ischemia and reperfusion. Brain Res 1984;304:9–22.
52. Peres M, Bourgeois D, Roussel S, et al. Two-dimensional 1H spectroscopic imaging for evaluating the local metabolic response to focal ischemia in the conscious rat. NMR Biomed 1992;5:11–19.
53. Bruhn H, Frahm J, Gyngell ML, Merboldt KD, Hanicke W, Sauter R. Cerebral metabolism in man after acute stroke: new observations using localized proton NMR spectroscopy. Magn Reson Med 1989;9:126–131.
54. Cvoro V, Wardlaw JM, Marshall I, Armitage PA, Rivers CS, Bastin ME, Carpenter TK, Wartolowska K, Farrall AJ, Dennis MS. Associations between diffusion and perfusion parameters, N-acetyl aspartate, and lactate in acute ischemic stroke. Stroke 2009;40:767–772.
55. Federico F, Simone IL, Lucivero V, Giannini P, Laddomada G, Mezzapesa DM, Tortorella C. Prognostic value of proton magnetic resonance spectroscopy in ischemic stroke. Arch Neurol 1998;55:489–494.
56. Ford CC, Griffey RH, Matwiyoff NA, Rosenberg GA. Multivoxel 1H-MRS of stroke. Neurology 1992;42:1408–1412.
57. Gideon P, Henriksen O, Sperling B, Christiansen P, Olsen TS, Jorgensen HS, Arlien-Soborg P. Early time course of N-acetylaspartate, creatine and phosphocreatine, and compounds containing choline in the brain after acute stroke. A proton magnetic resonance spectroscopy study. Stroke 1992;23:1566–1572.
58. Graham GD, Kalvach P, Blamire AM, Brass LM, Fayad PB, Prichard JW. Clinical correlates of proton magnetic resonance spectroscopy findings after acute cerebral infarction. Stroke 1995;26:225–229.
59. Pereira AC, Saunders DE, Doyle VL, Bland JM, Howe FA, Griffiths JR, Brown MM. Measurement of initial N-acetyl aspartate concentration by magnetic resonance spectroscopy and initial infarct volume by MRI predicts outcome in patients with middle cerebral artery territory infarction. Stroke 1999;30:1577–1582.
60. Lei H, Berthet C, Hirt L, Gruetter R. Evolution of the neurochemical profile after transient focal cerebral ischemia in the mouse brain. J Cereb Blood Flow Metab 2009;29:811–819.
61. Berthet C, Lei H, Gruetter R, Hirt L. Early predictive biomarkers for lesion after transient cerebral ischemia. Stroke 2011;42:799–805.
62. Mlynarik V, Kohler I, Gambarota G, Vaslin A, Clarke PG, Gruetter R. Quantitative proton spectroscopic imaging of the neurochemical profile in rat brain with microliter resolution at ultra-short echo times. Magn Reson Med 2008;59:52–58.
63. Hossmann KA, Schuier FJ. Experimental brain infarcts in cats. I. Pathophysiological observations. Stroke 1980;11:583–592.
64. Lin W, Venkatesan R, Gurleyik K, He YY, Powers WJ, Hsu CY. An absolute measurement of brain water content using magnetic resonance imaging in two focal cerebral ischemic rat models. J Cereb Blood Flow Metab 2000;20:37–44.
65. Macri MA, D'Alessandro N, Di Giulio C, Di Iorio P, Di Luzio S, Giuliani P, Esposito E, Pokorski M. Region-specific effects on brain metabolites of hypoxia and hyperoxia overlaid on cerebral ischemia in young and old rats: a quantitative proton magnetic resonance spectroscopy study. J Biomed Sci 2010;17:14.

66. van Zijl PC, Yadav NN. Chemical exchange saturation transfer (CEST): what is in a name and what isn't? Magn Reson Med 2011;65:927–948.

67. Segawa T, Kateb F, Duma L, Bodenhausen G, Pelupessy P. Exchange rate constants of invisible protons in proteins determined by NMR spectroscopy. Chembiochem 2008;9:537–542.

68. Paschen W, Djuricic B, Mies G, Schmidt-Kastner R, Linn F. Lactate and pH in the brain: association and dissociation in different pathophysiological states. J Neurochem 1987;48:154–159.

69. Stein WH, Moore S. Amino acid composition of beta-lactoglobulin and bovine serum albumin. J Biol Chem 1949;178:79–91.

70. Nisbet AD, Saundry RH, Moir AJ, Fothergill LA, Fothergill JE. The complete amino-acid sequence of hen ovalbumin. Eur J Biochem 1981;115:335–345.

71. Govindaraju V, Young K, Maudsley AA. Proton NMR chemical shifts and coupling constants for brain metabolites. NMR Biomed 2000;13:129–153.

72. Meresi GH, Cuperlovic M, Palke WE, Gerig JT. Pulsed field gradients in simulations of one- and two-dimensional NMR spectra. J Magn Reson 1999;137:186–195.

73. Young K, Matson GB, Govindaraju V, Maudsley AA. Spectral simulations incorporating gradient coherence selection. J Magn Reson 1999;140:146–152.